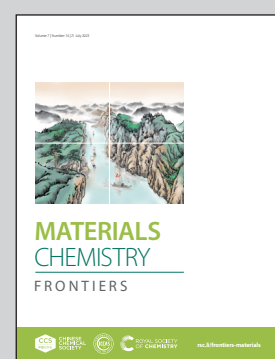


Showcasing research from Professor Sisi He's laboratory,  
School of Science, Harbin Institute of Technology  
(Shenzhen), Shenzhen, China.

Unveiling the effects of ions in the electric double layer on  
the carbon dioxide reduction reaction

This work reviews the recent advances in understanding  
the effects of cations and anions on determining the  
catalytic electrocatalytic mechanisms and performance of  
electrochemical carbon dioxide reduction reactions.

### As featured in:



See Sisi He et al.,  
*Mater. Chem. Front.*, 2023, **7**, 2750.

Registered charity number: 207890



CHINESE  
CHEMICAL  
SOCIETY



ROYAL SOCIETY  
OF CHEMISTRY

[rsc.li/frontiers-materials](http://rsc.li/frontiers-materials)



Cite this: *Mater. Chem. Front.*,  
2023, 7, 2750

## Unveiling the effects of ions in the electric double layer on the carbon dioxide reduction reaction

Fenglou Ni, Kangkang Jia, Yangyang Chen, Yunzhou Wen and Sisi He \*

As a potential approach to minimize carbon emissions, the electrocatalytic transfer of carbon dioxide ( $\text{CO}_2$ ) to valuable chemicals has attracted great attention. Since such a process takes place at the liquid/solid interface, the electrolyte plays a vital role in determining the catalytic performance. Particularly, the cations including alkali metal cations and organic cations, and/or anions of the electrolyte can greatly change the activity and selectivity of the  $\text{CO}_2$  reduction reaction ( $\text{CO}_2\text{RR}$ ). Here, we review the development of the electric double layer and recent advances in the understanding of cation effects and anion effects on their electrocatalytic mechanisms and performance. Insights into the behavior of cations and anions in the electric double layer and their various mechanistic impacts on the electrochemical reduction of  $\text{CO}_2$  are of critical importance in optimizing reaction conditions and designing reactors for the efficient conversion of  $\text{CO}_2$ . Finally, several challenges and outlook for better understanding and utilizing the electric double layer in the enhancement of the  $\text{CO}_2\text{RR}$  are proposed, and we hope that this review can provide guidance for the design of more efficient  $\text{CO}_2\text{RR}$  electrocatalysts.

Received 18th March 2023,  
Accepted 23rd May 2023

DOI: 10.1039/d3qm00277b

[rsc.li/frontiers-materials](http://rsc.li/frontiers-materials)

### 1. Introduction

The electrochemical reduction of carbon dioxide into valuable chemical commodities has significant potential to achieve the carbon-neutral goal while at the same time making full use of intermittent and renewable energy sources.<sup>1–3</sup> The development of catalysts, as a key factor in the  $\text{CO}_2\text{RR}$ , has been progressing

rapidly and tremendously in recent years.<sup>4–7</sup> Many strategies, such as adjusting the morphology,<sup>8</sup> chemical state,<sup>9,10</sup> surface facet,<sup>11</sup> and coordination structure<sup>12</sup> and introducing different elements,<sup>13,14</sup> have been applied to the design of highly active catalysts. Thus, near-unity faradaic efficiencies (FEs) for  $\text{CO}_2$  reduction to carbon monoxide (CO) and formate have been achieved on various catalysts, including metal, single-atom material, and molecular catalysts.<sup>15–22</sup> The FEs for  $\text{CO}_2$  reduction to multi-carbon products ( $\text{C}_{2+}$ ) are now above 70% on copper.<sup>23–29</sup> Besides, the electrodes and reactors also play significant roles in the  $\text{CO}_2\text{RR}$ .<sup>30,31</sup> Generally, there are two kinds of reactors, a conventional H-type reactor and a gas diffusion electrode (GDE) based flow-cell reactor. The H-type reactor has been widely used in fundamental research on the  $\text{CO}_2\text{RR}$ , as the dissolved  $\text{CO}_2$  concentration in the electrolyte mainly determines the current density (less than  $100 \text{ mA cm}^{-2}$  in most cases). But, using the GDEs in flow cell reactors,  $\text{CO}_2$  is able to directly reach the catalyst in the gas phase, greatly improving the mass transport of  $\text{CO}_2$  and thus achieving higher current density (more than  $1 \text{ A cm}^{-2}$ ).<sup>25,26</sup> Meanwhile, the high local alkalinity generated by high current densities can suppress the activity of the hydrogen evolution reaction (HER),<sup>28</sup> which further enhances the selectivity for the  $\text{CO}_2\text{RR}$ .<sup>27,32</sup>

While seeing the advances in designing  $\text{CO}_2\text{RR}$  catalysts and reactors, one may find that some major issues, *e.g.*, high overpotentials<sup>33</sup> and carbonate ( $\text{CO}_3^{2-}$ ) formation,<sup>34,35</sup> seem challenging to be addressed solely by the optimization of catalysts and reactors. Indeed, today's  $\text{CO}_2\text{RR}$  reactors suffer

School of Science, Harbin Institute of Technology (Shenzhen), University Town, Shenzhen, Guangdong, 518055, China. E-mail: [hesisi@hit.edu.cn](mailto:hesisi@hit.edu.cn)



Sisi He

*Sisi He is an Associate Professor at the Harbin Institute of Technology (Shenzhen) in China. She received her B.E. (2011), M.S. (2014) and PhD (2017) from Northeastern University, Tianjin University and Fudan University, respectively, and then worked as a postdoctoral fellow in Okinawa Institute of Science and Technology Graduate University, Japan and MacMaster University, Canada during 2018–2021. Her current interests focus on electrochemistry-related research areas including flexible sensor/energy storage and conversion platforms and electrocatalytic syntheses.*

Published on 26 May 2023. Downloaded on 2/16/2026 6:53:27 AM.

from large cell voltages above 3 V and huge additional energy costs due to the overpotential and  $\text{CO}_3^{2-}$  formation issues.<sup>27,36</sup> With more and more attention paid to the catalyst–electrolyte interface of the  $\text{CO}_2$ RR, mainly the electric double layer (EDL), the interplay between the local reaction microenvironment and the catalytic performance emerges as a new direction progressing the  $\text{CO}_2$ RR towards practical applications.<sup>37–39</sup>

Therefore, this review aims to briefly summarize the progress of the research on the role of an EDL in the  $\text{CO}_2$ RR. An EDL consists of catalyst surfaces, ions, and important intermediates and reactants, determining the selectivity and activity. We first narrate the classic theory of EDLs and their development history, then focus on outlining the effects of EDLs on the  $\text{CO}_2$ RR with the research toolkits for studying EDLs which were divided into two types, *i.e.*, cation effects and anion effects. Finally, we end this review by discussing the remaining challenges in understanding and utilizing EDLs to enhance  $\text{CO}_2$ RR performance.

## 2. The theory of EDLs

An EDL is a structure existing at a charged interface consisting of a fluid and an object (*e.g.*, a solid, a gas bubble, and a liquid droplet) exposed to the fluid.<sup>40</sup> In electrochemistry, the EDL can be understood in a simplified model having two parallel layers: one is the charged electrode surface and the other consists of counterions accumulated at a distance of a few nanometers to the surface.<sup>41</sup> This model is similar to a parallel-plate capacitor first proposed by Helmholtz.<sup>42</sup> The two plates, corresponding to the charged electrode and the accumulated counterions layer, define the Helmholtz layer. Within it, the differential capacitance is a constant, and the potential decreases linearly (Fig. 1a).

However, as observed by Gouy and Chapman, the capacitance of an EDL is positively proportional to the applied potential and the ionic concentration.<sup>43,44</sup> Thereby, the “Gouy-Chapman model” was proposed. This model describes that the equilibrium distribution of ions as a function of the distance to the surface follows the Maxwell-Boltzmann statistics. That is, the concentration of the counterions will progressively reduce to the bulk concentration at a certain distance. As a result, the interfacial potential exponentially decays away from the surface (Fig. 1b).

Combining the Helmholtz model and the Gouy-Chapman model, the Gouy-Chapman-Stern (GCS) model was obtained.<sup>45</sup> The GCS model proposed by Stern regarded ions as point charges. Later, this model was further modified by considering the solvation shells of ions and their specific adsorption on the electrode surface. Thus, this classical description of the EDL consists of three different regions (Fig. 1c): the inner Helmholtz plane (IHP),<sup>46</sup> the outer Helmholtz plane (OHP), and the diffusion layer. The IHP passes through the centers of the specifically adsorbed species. The OHP passes through the centers of solvated counterions (hydrated cations in the  $\text{CO}_2$ RR) accumulated at a distance closest to the surface. Finally, the diffusion layer refers to the region beyond the OHP. Within this EDL

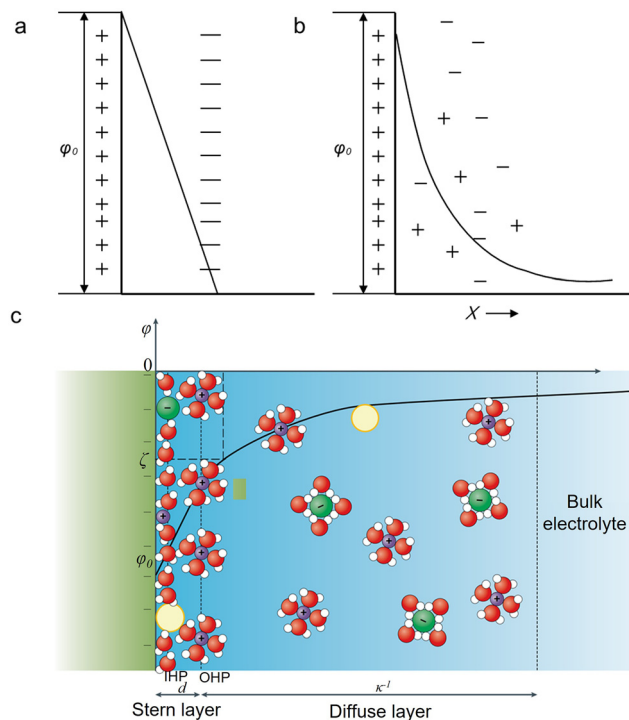


Fig. 1 Schematic description of different EDL models at a negatively charged electrode. (a) The Helmholtz model. (b) The Gouy-Chapman model. (c) The Gouy-Chapman-Stern model.<sup>40</sup> The yellow, green, purple, red, and white spheres represent neutral species, the anions, the cations, oxygen and hydrogen. Reproduced from ref. 40 with permission from the Springer Nature, copyright 2021.

structure, the electrode surface, ions, and electrically neutral species play essential roles in determining the activity and selectivity for electrochemical processes.<sup>47,48</sup> For the  $\text{CO}_2$ RR, as documented in the literature, cations and anions strongly affect the catalytic performance.<sup>38,49–51</sup> Thus, in the next section, we will elaborate on how the above factors tune the  $\text{CO}_2$ RR performance.

## 3. Mechanisms of cation effects

In 1969, Paik *et al.* found that cations impacted the  $\text{CO}_2$ RR kinetics and the current density increased in the order  $\text{Li}^+ < \text{Na}^+ < (\text{Et})_4\text{N}^+$  at a given potential on the mercury electrodes.<sup>52</sup> Later, Hori *et al.* observed that increasing the cation size (crystal ionic size) from  $\text{Li}^+$  to  $\text{Cs}^+$  could enhance the selectivity of  $\text{C}_{2+}$  products on Cu electrodes.<sup>53</sup> Since then, lots of research has been conducted to further deeply investigate the effect of monovalent alkali cations, including  $\text{Li}^+$ ,  $\text{Na}^+$ ,  $\text{K}^+$ ,  $\text{Rb}^+$  and  $\text{Cs}^+$ , on the  $\text{CO}_2$ RR. Moreover, multivalent cations<sup>54</sup> and organic cations<sup>55</sup> are also used to improve the activity and selectivity, and explore the mechanisms of cation effects. To date, several main hypotheses, including (1) the specific adsorption of cations,<sup>53</sup> (2) the hydrolysis of hydrated cations,<sup>56</sup> (3) the interactions between the intermediates and the electric field or cations,<sup>57,58</sup> (4) the suppression of the HER,<sup>59</sup> and (5) other effects including multivalent or organic cations have been

proposed to interpret the above disparity. With a better understanding by combining the density functional theory (DFT) calculations and advanced characterization methods, the evolution of these assumptions is still ongoing.

### 3.1. Specific adsorption of cations

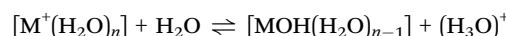
Murata and Hori first proposed that the potential change at the OHP led to the differences in selectivity and activity among different cations.<sup>53,60</sup> Such a potential change is highly related to the hydration extent of cations, which further affects the local pH. Smaller cations (e.g.,  $\text{Li}^+$ ) are strongly hydrated, thus hindering their specific adsorption on the electrode surface. In contrast, larger cations (e.g.,  $\text{K}^+$  and  $\text{Cs}^+$ ) with a lower hydration number are able to adsorb more easily on the surface. As the specific adsorption of cations gave rise to a positive shift of the OHP potential, the electrode potential became more positive for larger cations at a constant current density.<sup>61</sup> Meanwhile, the concentration of hydrogen anions ( $\text{H}^+$ ) decreased in the electrolytes containing larger cations, resulting in higher pH values at the OHP and thereby increasing the  $\text{C}_2/\text{C}_1$  product ratio. Besides, specifically adsorbed larger cations have also been theoretically proven to promote the C-C coupling through stabilizing the \*CHO intermediates.<sup>62</sup> More recently, similar cation effects were also observed in the  $\text{CO}_2\text{RR}$  on silver GDEs, where an enhancement of CO FE was achieved with increasing cation size.<sup>63</sup> This improvement was also rationalized by the interplay between the hydration level of cations and the extent of cations' special adsorption. Furthermore, surface-enhanced infrared absorption spectroscopy (SEIRAS) was experimentally conducted to probe the asymmetric  $\text{CH}_3$  deformation band of tetramethylammonium (methyl<sub>4</sub>N<sup>+</sup>) by Vincent *et al.* and they observed the specific adsorption of alkali cations on Au electrodes.<sup>64</sup> Compared with the pure methyl<sub>4</sub>N<sup>+</sup> electrolyte, a negative-going band at  $\sim 1842 \text{ cm}^{-1}$  appeared after the addition of cations, which is due to the displacement of specifically adsorbed methyl<sub>4</sub>N<sup>+</sup> by cations. Meanwhile, through integrating the area of the above band, the surface coverage of specifically adsorbed cations increased in the order  $\text{Li}^+ < \text{Na}^+ < \text{K}^+ < \text{Cs}^+$ , indicating that cations with softer hydration shells are more likely to specifically adsorb on the surface.

However, Strmcnik *et al.* and Milles *et al.* argued that the specific adsorption of hydrated cations failed to account for the above-observed impact, based on the DFT calculations.<sup>65,66</sup> The equilibrium potentials for the specific adsorption of alkali cations are more negative than  $-2.4 \text{ V}$  vs. the normal hydrogen electrode (NHE) on Au, suggesting that the specific adsorption of cations may not occur at commonly applied potentials of the  $\text{CO}_2\text{RR}$ .

So far, whether cations adsorb specifically or electrostatically below the potential of zero charge is still ambiguous in the  $\text{CO}_2\text{RR}$ . But most of the recent studies on the  $\text{CO}_2\text{RR}$  tended to accept that cations accumulate near the electrode surface *via* non-covalent interactions rather than specific adsorption.<sup>55–58</sup>

### 3.2. Hydrolysis of hydrated cations

Recently, another hypothesis about cation effects in the  $\text{CO}_2\text{RR}$  was proposed by Singh and co-workers, attributing this to the buffering capacity of the hydrolysis of hydrated cations near the cathode.<sup>56</sup>



The  $\text{p}K_a$  of the above reaction at the electrode surface is

$$\text{p}K_a = -A \left( \frac{z^2}{r_{\text{M-O}}} + 2\pi\sigma z r_{\text{H-EI}} \left( \sqrt{1 + \frac{r_{\text{M-O}}^2}{r_{\text{H-EI}}^2}} \right) \right) + B$$

where  $z$  and  $\sigma$  are the effective charges on the hydrated cation and the surface charge density on the cathode, respectively;  $r_{\text{M-O}}$  and  $r_{\text{H-EI}}$  are the distance between the centers of the O atom in the hydration shell and the cation and the distance from the electrode surface to the center of the hydrogen atom of bound water, respectively; and  $A$  and  $B$  are the empirical constants. The first item in the parenthesis represents one component of the  $\text{p}K_a$  which is due to the interactions between cations and water molecules in the hydration sphere. Moreover, the O-H bonds of water molecules within the OHP are further polarized by the cation-induced interfacial electrostatic field, which is described by the second term.

In light of the above equation, the calculated  $\text{p}K_a$  values for different hydrated cations were comparable in the bulk electrolytes, but decreased near the electrodes in the sequence of  $\text{Li}^+ (11.64) > \text{Na}^+ (10.26) > \text{K}^+ (7.95) > \text{Rb}^+ (6.97) > \text{Cs}^+ (4.31)$  at  $-1 \text{ V}$  *versus* the reversible hydrogen electrode (RHE). Thus,  $\text{Cs}^+$  displayed a stronger buffering ability, offering more protons to counteract the increasingly local hydroxide anions ( $\text{OH}^-$ ) and thereby maintaining the local pH close to that in the bulk ( $\text{pH} = 7$ ) in comparison with the case of  $\text{Li}^+$ .<sup>67</sup> This neutral microenvironment impeded the reaction of  $\text{CO}_2$  molecules with  $\text{OH}^-$  to produce bicarbonate ( $\text{HCO}_3^-$ ) or  $\text{CO}_3^{2-}$  anions, thus enhancing the local concentration of  $\text{CO}_2$  available for the reduction (Fig. 2a). Clearly, according to the calculation results, this pronounced effect promoted the FE of CO on Ag cathodes from 55.8% in  $\text{Li}^+$  to 90.2% in  $\text{Cs}^+$ . Meanwhile, such a noticeable improvement also occurred in the  $\text{C}_2/\text{C}_1$  selectivity ratio over Cu electrodes.

However, this theoretical buffering capability of cations was overestimated, when compared with the experimental results. Cuesta *et al.* noted that the pH at the electrode surface could be probed using SEIRAS.<sup>68</sup> As the concentration equilibrium between  $\text{CO}_2$  and  $\text{HCO}_3^-$  species is related to the concentration of  $\text{H}^+$ , the pH change at the interface during the  $\text{CO}_2\text{RR}$  can be determined by the ratio of the integrated intensity between the  $\text{CO}_2$  and  $\text{HCO}_3^-$  bands. As shown in Fig. 2b, while the local pH decreased with increasing cation size, the experimental pH values for larger cations were much higher than those obtained using DFT calculations. Moreover, similar results were obtained on a rotating ring-disc electrode as well.<sup>68–70</sup> Liu *et al.* developed a considerably sensitive pH sensor by using the redox couple of 4-hydroxylaminothiophenol (4-HATP)/4-nitrosothiophenol

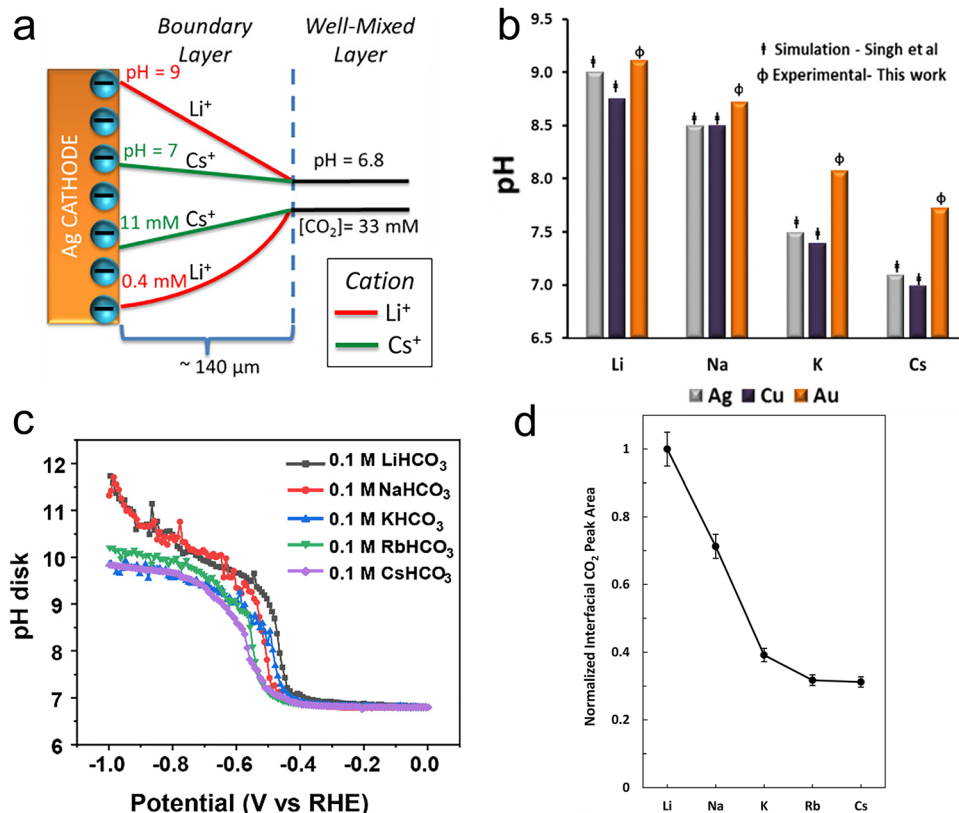


Fig. 2 (a) Profiles of pH and CO<sub>2</sub> concentrations as a result of the cations' pK<sub>a</sub> values on Ag electrodes.<sup>56</sup> Reproduced from ref. 56 with permission from the American Chemical Society, copyright 2016. (b) Steady-state pH values at the interface in CO<sub>2</sub>-saturated 0.05 M carbonate solutions at -1.0 V vs. RHE on Au electrodes in comparison with the results from Singh *et al.*'s calculations.<sup>68</sup> Reproduced from ref. 68 with permission from the American Chemical Society, copyright 2017. (c) The interfacial pH values under various potentials in 0.1 M CO<sub>2</sub>-saturated electrolytes with different cations.<sup>70</sup> Reproduced from ref. 70 with permission from the Royal Society of Chemistry, copyright 2023. (d) The interfacial CO<sub>2</sub> concentration was determined by measuring the areas of the dissolved CO<sub>2</sub> band in different cations and then normalizing the band areas with that of Li<sup>+</sup>.<sup>71</sup> Reproduced from ref. 71 with permission from the American Chemical Society, copyright 2020.

(4-NSTP), and combined this sensor with a rotating ring-disc electrode system to directly estimate the interfacial pH of gold electrodes.<sup>70</sup> As illustrated in Fig. 2c, the interfacial pH decreases with increasing the cation size from Li<sup>+</sup> to Cs<sup>+</sup>. However, the trend and the cations' buffering ability are both less pronounced compared to the calculated theoretical results. On the other hand, since the peak potential for the oxidation of CO on the Pt ring electrode is sensitive to the local pH, and shifts by  $-86 \pm 2$  mV pH<sup>-1</sup>, such a potential change can quantitatively describe deviations in the local pH among cations.<sup>69</sup> The local basicity followed the trend Li<sup>+</sup> > Na<sup>+</sup> > K<sup>+</sup> > Cs<sup>+</sup> under the same CO<sub>2</sub>RR conditions in Singh *et al.*'s work, but the difference in local pH values between Li<sup>+</sup> and Cs<sup>+</sup> electrolytes was only 0.28 at a current density of 5 mA cm<sup>-2</sup>, and 0.74 even at 15 mA cm<sup>-2</sup>. Such a small difference in pH values between Li<sup>+</sup> and Cs<sup>+</sup> may not be considered the reason for the activity improvement.

Instead of boosting the interfacial CO<sub>2</sub> concentration by increasing the cation size according to previous theoretical calculations, Xu *et al.* found the opposite trend by using attenuated total reflection surface-enhanced infrared absorption spectroscopy (ATR-SEIRAS).<sup>71</sup> As displayed in Fig. 2d, while

the integrated area of the dissolved CO<sub>2</sub> band decreased by 69% from Li<sup>+</sup> to Cs<sup>+</sup>, the partial current density of CO increased more than 10 times. This suggests that the local CO<sub>2</sub> concentration mainly depended on the consumption rate, specifically the reaction rate, rather than on the buffering capacity of hydrated cations. Thus, a lower local CO<sub>2</sub> concentration was obtained in electrolytes containing larger cations, since they accelerated the rate of the CO<sub>2</sub>RR.

### 3.3. Interactions between intermediates and the electric field or cations

The above two hypotheses do not consider the effect of an electric field on the energetics of the uncharged species which have a large dipole moment and/or polarizability. As the electric field over 0.1 V Å<sup>-1</sup> could vary the energies of molecular orbitals of adsorbates, the electrostatic forces would markedly alter the adsorption free energies of intermediates and the activation barrier, thus changing the activity and selectivity for electrochemical reactions.<sup>72</sup> Through introducing an explicit model of the electrochemical interface, Nørskov *et al.* investigated the effect of the electric field resulting from hydrated cations and their corresponding image charges at the interface in the

CO<sub>2</sub>RR on Ag(111) electrodes.<sup>57</sup> With K<sup>+</sup>, an applied electric field of  $-1$  V Å<sup>-1</sup> significantly lowers the free energy of the intermediate \*CO<sub>2</sub> and thus stabilizes this key intermediate. On Cu electrodes, the surface intermediates with strong dipole moments (e.g., \*CO<sub>2</sub>, \*CO, \*OCCO) could also be stabilized by the cation-induced electrostatic field.<sup>73,74</sup>

Furthermore, the interfacial field strength varies with different cations, which impacts the extent of the stabilization effect on the dipolar and polarizable intermediates and further gives rise to pronounced differences between cations.<sup>73</sup> Increasing the cation size leads to higher electric field strength, which can greatly stabilize the intermediates. Besides, as the intermediate \*CO has a larger dipole moment than \*CHO, the key intermediate for forming methane, larger cations are more inclined to enhance the formation rates of C<sub>2</sub> products than C<sub>1</sub> products on Cu electrodes (Fig. 3a). Perez-Gallent *et al.* also noted that the cation-induced field could dramatically stabilize the C<sub>2</sub> intermediates with respect to C<sub>1</sub> species in the CO reduction reaction, resulting in an increasing trend of the selectivity towards ethylene with the increase of the cation size.<sup>75</sup> To interpret the above changes, the enhancement of the electric field intensity was attributed to the accumulation of more cations at the OHP, determined by a few factors, including (i) the driving force for cations,<sup>73</sup> (ii) the repulsion effect,<sup>76</sup> and (iii) the effect of volume exclusion.<sup>77</sup>

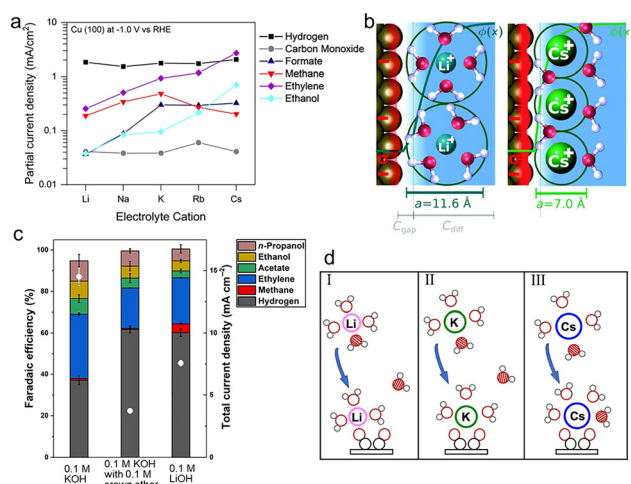


Fig. 3 (a) Partial current densities for each product of CO<sub>2</sub> reduction on Cu(100) at  $-1.0$  V vs. RHE as a function of the electrolyte cation.<sup>73</sup> Reproduced from ref. 73 with permission from the American Chemical Society, copyright 2017. (b) The repulsion between solvated cations at the OHP reduces the local concentrations of cations, the EDL field, and the surface charge density ( $\sigma$ , depicted by the red region). The diameters for solvated Li<sup>+</sup> and Cs<sup>+</sup> are 11.6 Å and 7.0 Å, respectively.<sup>76</sup> Reproduced from ref. 76 with permission from the Royal Society of Chemistry, copyright 2019. (c) FEs for each product and total current densities (white dots) obtained on Cu electrodes at  $-0.7$  V vs. RHE in 0.1 M potassium hydroxide (KOH) with and without 0.1 M crown ether, and 0.1 M lithium hydroxide (LiOH), respectively.<sup>82</sup> Reproduced from ref. 82 with permission from the Science Advances is the American Association for the Advancement of Science, copyright 2020. (d) Schematic diagrams of the coordination of hydrated cations Li<sup>+</sup>(I), K<sup>+</sup>(II), and Cs<sup>+</sup>(III) with water and the intermediate \*OCCO during the CO coupling process.<sup>85</sup> Reproduced from ref. 85 with permission from the American Chemical Society, copyright 2021.

In terms of the driving force, it would be enhanced by increasing the cation size, thus improving the movement of cations to be at the OHP from the bulk electrolyte and leading to a higher concentration of larger cations near the electrode. Especially, the driving force for Cs<sup>+</sup> is more favorable by  $\sim 1$  eV compared to that for Li<sup>+</sup>.<sup>73</sup> This result can be experimentally proved by analyzing the peak frequency of the C≡O stretch band of surface-adsorbed CO using time-resolved and surface-sensitive infrared spectroscopy.<sup>78</sup> With increasing cation size, the C≡O stretch frequency shifted to lower energies, suggesting that surface-adsorbed CO molecules experienced a stronger interfacial field.

As for the repulsion effect, Ringe *et al.* noted that larger cations with a smaller hydrated cation radius displayed smaller repulsion and therefore became more concentrated at the OHP by combining the size-modified Poisson–Boltzmann theory and *ab initio* simulation (Fig. 3b).<sup>76</sup> The effective radii of hydrated cations follow the order Li<sup>+</sup> (5.8 Å) > Na<sup>+</sup> (5.2 Å) > K<sup>+</sup> (4.1 Å) > Rb<sup>+</sup> (3.9 Å) > Cs<sup>+</sup> (3.5 Å),<sup>79,80</sup> indicating that the highest concentration of Cs<sup>+</sup> is formed close to the electrode. Moreover, due to the volume exclusion, the migration of hydrated cations to the OHP would reach the steric limit with increasing applied potentials, further forming a condensed layer.<sup>77</sup> The higher concentration of larger cations at the OHP was observed with a thinner layer, which was also in favor of the mass transport of CO<sub>2</sub> to the electrode surface.

According to the GCS model, the variation of the electric field strength among different cations can be experimentally quantified by measuring the Stark tuning rate, which is dependent on the effective size of hydrated cations.<sup>81,82</sup> The Stark tuning rate increases from 29 to 39 cm<sup>-1</sup> V<sup>-1</sup> from Li<sup>+</sup> to K<sup>+</sup>, and stabilizes at 39 to 41 cm<sup>-1</sup> V<sup>-1</sup> from K<sup>+</sup> to Cs<sup>+</sup>. Compared with Li<sup>+</sup>, the relatively larger Stark tuning rates correspond to higher field intensity, as well as smaller effective sizes of hydrated cations following the order Li<sup>+(H<sub>2</sub>O)x</sup> > Na<sup>+(H<sub>2</sub>O)x</sup> > K<sup>+(H<sub>2</sub>O)x</sup>  $\sim$  Rb<sup>+(H<sub>2</sub>O)x</sup>  $\sim$  Cs<sup>+(H<sub>2</sub>O)x</sup>. Moreover, smaller cations like Li<sup>+</sup> have a thicker hydration shell with more than one layer of water molecules, still effectively impacting the reactions at the interface.

Besides the above-mentioned intermediate-field medium-range interactions, the short-range interactions between intermediates and hydrated cations may have a similar stabilization effect as well. For instance, the FE for C<sub>2+</sub> products increased from Li<sup>+</sup> to K<sup>+</sup> and kept primarily unchanged from K<sup>+</sup> to Cs<sup>+</sup>, which was in line with the trend of electric field strength.<sup>82</sup> However, the current density increased monotonically with the cation size. Due to the observed similar peak positions and lineshapes of adsorbed CO with K<sup>+</sup> and Cs<sup>+</sup> from the ATR-SEIRAS spectra, these cations showed comparable interactions with the adsorbed CO. Furthermore, chelating K<sup>+</sup> with the crown ether would result in the same Stark tuning rate as that of hydrated Li<sup>+</sup>, demonstrating that the chelated K<sup>+</sup> and hydrated Li<sup>+</sup> had similar field strength and effective sizes. The comparable field strength resulted in a similar product distribution, but the current density for Li<sup>+</sup> was 2 times higher than that for the chelated K<sup>+</sup> (Fig. 3c). The above results

manifested that the reaction rate was directly related to the nature and structure of the cation. The differences between larger cations could be due to the increasingly looser association with the hydration shell. Furthermore, at the same pH, increasing the concentration of  $\text{Na}^+$  from 0.1 to 1.0 M dramatically promoted the formation of  $\text{C}_{2+}$  products without changing the field strength.<sup>83</sup> This improvement demonstrates that the nature of cations plays a significant role in tuning the reactivity and selectivity as well.

Such an effect of the nature of cations was further proved using theoretical calculations. By integrating the *ab initio* molecular dynamics simulations with the slow-growth sampling method, Qin *et al.* observed that the presence of  $\text{K}^+$  cations facilitated the rate-determining  $\text{CO}_2$  activation step by the coordination interactions.<sup>84</sup> Through coordinating with  $\text{CO}_2$  molecules to form a cation– $\text{CO}_2$  complex, cations favor the stabilization of the  $^*\text{CO}_2^-$  intermediates by  $\sim 0.5$  eV than the solvation of water molecules, hence initiating the  $\text{CO}_2$ RR.<sup>58</sup> The average  $\text{CO}_2$  coordination numbers obtained from *ab initio* molecular dynamics simulations are  $0.1 \pm 0.3$ ,  $0.9 \pm 0.2$ ,  $0.9 \pm 0.4$ ,  $1.3 \pm 0.5$  for  $\text{Li}^+$ ,  $\text{Na}^+$ ,  $\text{K}^+$  and  $\text{Cs}^+$ , respectively. Due to its hard solvation shell,  $\text{Li}^+$  poorly coordinates with  $\text{CO}_2$ . In contrast, larger cations with a softer hydration shell can not only strongly interact with  $\text{CO}_2$ , but also become more concentrated at the OHP, accounting for the activity trend  $\text{Cs}^+ > \text{K}^+ > \text{Na}^+ > \text{Li}^+$  in the  $\text{CO}_2$ RR. Moreover, the decrease of the O–C–O angle from a linear  $180^\circ$  to below  $140^\circ$  caused by the cation– $\text{CO}_2$  complex, and the enhancement of the electron transfer from the interface to  $\text{CO}_2$  might also promote the stabilization effect. Another cation–OCCO complex has also been found to improve the conversion of  $\text{CO}_2$  to  $\text{C}_2$  products.<sup>85</sup> As displayed in Fig. 3d, compared to  $\text{Li}^+$ , larger cations  $\text{K}^+$  and  $\text{Cs}^+$  would get coordinated with two oxygen atoms in the intermediates  $^*\text{OCCO}$  simultaneously, which made the cation–intermediate complex more stable.

### 3.4. Suppression of the HER

As a major competing reaction during the  $\text{CO}_2$ RR, the HER significantly affects the selectivity of main products.<sup>86</sup> Thus, the suppression of the HER is vital to improve the conversion of  $\text{CO}_2$ . In the alkaline and neutral electrolytes, high  $\text{OH}^-$  concentrations at the interface greatly suppress the formation of  $\text{H}_2$ .<sup>28,87</sup> However,  $\text{OH}^-$  reacts with  $\text{CO}_2$  to form  $\text{CO}_3^{2-}$ , drastically reducing the local concentration of  $\text{CO}_2$  and its utilization efficiency.<sup>88–90</sup> Such an issue could be avoided by using acidic electrolytes, while the HER can be suppressed by the addition of cations.<sup>91,92</sup> For instance, nearly 100% FE of hydrogen was obtained on Au electrodes in  $\text{CO}_2$ -saturated 0.1 M perchloric acid ( $\text{HClO}_4$ ) solutions ( $\text{pH} = 1$ ), while an 80% FE of CO was achieved in  $\text{CO}_2$ -saturated 0.1 M potassium perchlorate ( $\text{KClO}_4$ ) solutions ( $\text{pH} = 3$ ).<sup>93</sup> Moreover, the efficient reduction of  $\text{CO}_2$  on Cu electrodes was reported in mixed electrolytes containing 1 M phosphoric acid ( $\text{H}_3\text{PO}_4$ ) and 3 M potassium chloride (KCl).<sup>92</sup> More recently, single-pass  $\text{CO}_2$  utilization efficiencies of 85% for  $\text{CO}_2$  to CO at  $600 \text{ mA cm}^{-2}$  and 60% for  $\text{CO}_2$  to  $\text{C}_{2+}$  at  $500 \text{ mA cm}^{-2}$  under acidic conditions,

respectively, were achieved, which greatly reduced the  $\text{CO}_2$  loss.<sup>94,95</sup> However, the mechanism of the cation suppression effect is still unclear.

The HER consists of two pathways, the reduction of protons ( $2\text{H}^+ + 2\text{e}^- \rightarrow \text{H}_2$ ) and the reduction of water ( $2\text{H}_2\text{O} + 2\text{e}^- \rightarrow \text{H}_2 + 2\text{OH}^-$ ).<sup>96–98</sup> As the proton reduction has an earlier onset potential than water reduction, the water reduction will become the major reaction by replacing the proton reduction under more negative potentials.<sup>99</sup> Gu *et al.* noticed that cations could suppress the proton reduction under the potentials more positive than the onset potential for the water reduction.<sup>59</sup> In pure trifluoromethanesulfonic acid (HOTf), no limiting current density of the proton reduction was observed. In contrast, with the addition of 0.4 M potassium trifluoromethanesulfonate (KOTf), a plateau of limiting current density appeared at  $-0.6 \text{ V}$  vs. the standard hydrogen electrode (SHE), which was due to the mass transport limitation of hydronium. Thus, in comparison with the  $\text{K}^+$ -free medium, hydrated cations at the OHP impeded the migration of hydronium ions toward the electrode, thereby decreasing the concentration of hydronium ions near the electrode. Through a further quantitative study, the identity of cations hardly impacted the plateau current density.<sup>100</sup> Meanwhile, increasing the concentration of cations, especially when it is higher than that of  $\text{H}^+$ , would substantially suppress the migration rate and the diffusion rate of  $\text{H}^+$ , and further restrain the HER.

Furthermore, the cations also highly affect the surface coverage of protons, further the activity of the HER. Xu *et al.* noticed that the proton adsorption was energetically unfavored in  $\text{K}^+$  compared to that in  $\text{Na}^+$ , owing to the higher orbital sensitivity and a stronger preference in the binding of  $\text{K}^+$  ions.<sup>101</sup> Thus, the  $\text{H}_2$  FE largely decreased from 73% ( $\text{Na}^+$ ) to 24% ( $\text{K}^+$ ). Additionally, due to the competitive adsorption of cations, increasing the concentration of cations could markedly decline the local concentration of protons near electrodes.<sup>102</sup> Such competition could suppress the HER and offer more local interactions to stabilize the intermediates  $^*\text{OCOH}$ , ultimately improving the efficient conversion of  $\text{CO}_2$ .

### 3.5. Other effects (multivalent cations and organic cations)

Apart from alkali cations, multivalent cations and ionic surfactants can also promote the  $\text{CO}_2$ RR, according to recent studies.<sup>54,103</sup> As multivalent cations having larger surface charges could improve the interfacial electric field strength, the cations including  $\text{Ba}^{2+}$  and  $\text{La}^{3+}$  displayed up to 2 orders of magnitude higher activity for the production of CO than  $\text{Cs}^+$ .<sup>76</sup> Such an acceleration effect was also observed on the rate of the  $\text{CO}_2$ RR over the Cu–Sn–Pb alloy electrodes.<sup>104</sup> The reaction rate in the electrolyte containing  $\text{La}^{3+}$  was 2 times higher than that in the case of  $\text{Na}^+$  at a lower overpotential ( $-0.65 \text{ V}$  vs.  $\text{Ag}/\text{AgCl}$ ).

To explicitly unravel the effect of multivalent cations, more dilute electrolytes (2 mM  $\text{M}^{n+}$  =  $\text{Li}^+$ ,  $\text{Cs}^+$ ,  $\text{Be}^{2+}$ ,  $\text{Mg}^{2+}$ ,  $\text{Ca}^{2+}$ ,  $\text{Ba}^{2+}$ ,  $\text{Al}^{3+}$ ,  $\text{Nd}^{3+}$ , and  $\text{Ce}^{3+}$ ; bulk  $\text{pH} = 3$ ) were used to minimize the possible deposition including oxides and hydroxides. As shown in Fig. 4a, Monteiro *et al.* found that the cation acidity, determining the accumulation of cations at the OHP and water

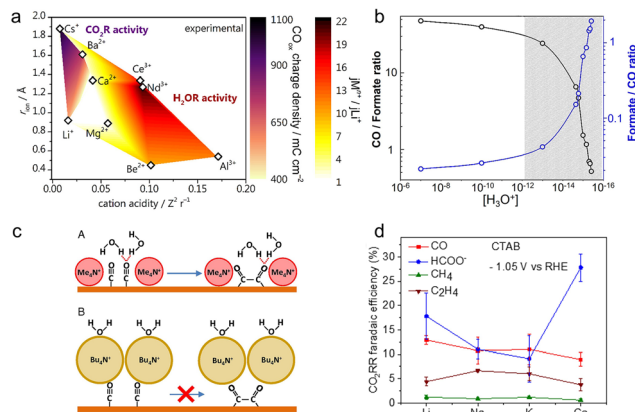


**Fig. 4** (a) The color map of the  $\text{CO}_2\text{RR}$  activity (purple shades) and HER activity (red shades) at high potentials as a function of cation acidity and cationic radius.<sup>54</sup> Reproduced from ref. 54 with permission from the American Chemical Society, copyright 2022. (b) The CO/formate ratio and formate/CO ratio at different concentrations of hydronium.<sup>106</sup> Reproduced from ref. 106 with permission from the American Chemical Society, copyright 2018. (c) The schematic of the CO coupling mechanism in the presence of methyl<sub>4</sub>N<sup>+</sup> and butyl<sub>4</sub>N<sup>+</sup>.<sup>103</sup> Reproduced from ref. 103 with permission from the Proceedings of the National Academy of Sciences of the United States of America, copyright 2019. (d) FEs for main products in the presence of CTAB and different cations at  $-1.05\text{ V}$  vs RHE.<sup>112</sup> Reproduced from ref. 112 with permission from the American Chemical Society, copyright 2020.

dissociation kinetics, affected the activities of the HER and  $\text{CO}_2\text{RR}$ .<sup>54</sup> On the one hand, as the activation barrier of water dissociation decreased with cation acidity, the weakly hydrated trivalent cations greatly increased the reaction rate of water reduction. Meanwhile, the softly hydrated cations including Ba<sup>2+</sup> and Nd<sup>3+</sup> could increasingly accumulate at the OHP and further accelerate the water reduction, due to the minimal repulsion. As for the  $\text{CO}_2\text{RR}$ , the short-range interactions generated by coordination between cations and the  $^{*}\text{CO}_2^-$  species could stabilize this intermediate, hence promoting the  $\text{CO}_2$  reduction. Therefore, at low potentials where the proton reduction reaction mainly takes place, more CO can be produced with increasing cation acidity, since the proton reduction is independent of the cation identity. In contrast, at high potentials, the activity for CO increased in the order  $\text{Ca}^{2+} < \text{Li}^+ < \text{Ba}^{2+} < \text{Cs}^+$ , as acidic cations extremely promoted the water reduction. In consequence, the interplay between the specific cation-intermediate interactions, the concentration of cations at the OHP, and the activity for water reduction should be taken into account for the investigation of the cation effect.

In contrast to the above promotion effect, Bhargava *et al.* noticed that multivalent cations hindered the reaction rate and selectivity for CO production.<sup>105</sup> Compared to monovalent cations, multivalent cations would impede the  $\text{CO}_2$  adsorption on the catalyst surface by blocking the active sites with *in situ* generated deposits including hydroxide, oxide, and carbonate. But this research was conducted in the electrolytes with a high concentration of cations (3 M) under high current densities, which led to a higher local pH value. This may be a possible reason for the reverse trend.

Hydronium within the double layer can switch product selectivity on Ag electrodes by altering the activation barrier for the hydrogenation of the intermediate  $^{*}\text{CO}_2^-$ .<sup>106</sup> Compared to the formation of  $^{*}\text{COOH}$ , the intermediate for producing CO, the activation energy barrier for forming  $^{*}\text{CHO}$ , and the intermediate for producing formate significantly dropped in the absence of hydronium. In the experiment, drastically reducing the local concentration of hydronium could hugely contribute to the switch of the reaction pathway from CO<sub>2</sub> to formate, achieving  $\sim 60\%$  FE of formate in 11 M KOH (Fig. 4b).

Specially, for the reduction of CO<sub>2</sub> to ethylene, the change in its selectivity correlates with the hydrogen bonding between the interfacial water and the CO dimer, rather than the strength of the cation-induced electric field.<sup>103</sup> Under the experimental conditions, the field strength had a negligible effect on the adsorption energy of CO on Cu, although the sizes of quaternary alkyl ammonium cations follow the order methyl<sub>4</sub>N<sup>+</sup> < ethyl<sub>4</sub>N<sup>+</sup> < propyl<sub>4</sub>N<sup>+</sup> < butyl<sub>4</sub>N<sup>+</sup>. Using SEIRAS, a sharp band was observed for the electrolytes containing methyl<sub>4</sub>N<sup>+</sup> and ethyl<sub>4</sub>N<sup>+</sup>, which was due to the hydrogen bonding of water to the terminal oxygen of adsorbed CO. Such interactions tended to stabilize the CO dimer and facilitate the formation of ethylene. But, due to the larger size and more hydrophobic nature, propyl<sub>4</sub>N<sup>+</sup> and butyl<sub>4</sub>N<sup>+</sup> effectively displaced water molecules from the interface. This displacement further led to the disruption of the interaction between the adsorbed CO and water, thus hindering CO dimerization (Fig. 4c). This difference can account for the production of ethylene only in methyl<sub>4</sub>N<sup>+</sup>- and ethyl<sub>4</sub>N<sup>+</sup>-containing electrolytes.

Introducing the organic cation of cetyltrimethylammonium bromide (CTAB) to the electrolytes can increase the rate of the  $\text{CO}_2\text{RR}$  and suppress the HER.<sup>108</sup> With the presence of CTAB in 0.1 M sodium bicarbonate (NaHCO<sub>3</sub>), the FE of H<sub>2</sub> approximately dropped by half, while the formate selectivity reaches almost 50% at  $-0.6\text{ V}$  vs. RHE.<sup>109</sup> Besides, increasing the concentration and chain length of CTAB could further improve the selectivity of CO and formate, and suppress the HER. According to the electrochemical impedance spectroscopy (EIS) study, the double layer capacitance value was lower in the presence of CTAB, which was attributed to the displacement of hydronium and hydrated Na<sup>+</sup> cations<sup>109</sup> and the formation of an ordered structure of CTAB enhancing the electron transfer at the interface.<sup>110</sup> This ordered surfactant assembly would repel isolated water near the interface and hinder the tendency of hydrogen atoms of local water molecules to approach the interface.<sup>110</sup> Combined with the depletion of the local proton source, both factors significantly inhibited the HER. At the same time, the CTAB at the interface disturbed the binding configuration of CO, shifting the CO band to a lower frequency, further increasing the CO surface coverage, and thus enhancing the activity of the  $\text{CO}_2\text{RR}$ .<sup>111</sup>

The presence of CTAB disfavored the formation of C<sub>2</sub> products but improved the formation of formate.<sup>112</sup> In Fig. 4d, the activity and selectivity for the  $\text{CO}_2\text{RR}$  were virtually independent of the identity of cations (Li<sup>+</sup>, Na<sup>+</sup> and K<sup>+</sup>) with CTAB. But an unexpected enhancement in formate selectivity was observed in

the presence of  $\text{Cs}^+$  and CTAB, while the selectivity for ethylene significantly dropped compared to the CTAB-free  $\text{Cs}^+$  electrolytes. Due to its hydrophobicity, the CTAB inhibited the C–C bond formation by disturbing the hydrogen bonding, reducing the formation of  $\text{C}_{2+}$  products. Meanwhile,  $\text{Cs}^+$  with a smaller hydrated size formed a more compact layer, thereby more easily displacing partial CTAB than other cations, leading to a higher formate FE.

## 4. Mechanisms of the anion effect

According to the buffer capacity, anions can be divided into two types: buffering anions ( $\text{HCO}_3^-$ ,  $\text{CO}_3^{2-}$ , and  $\text{H}_2\text{PO}_4^-$ ) and non-buffering anions ( $\text{Cl}^-$ ,  $\text{Br}^-$ ,  $\text{I}^-$ ,  $\text{ClO}_4^-$ ,  $\text{SO}_4^{2-}$ , and  $\text{OH}^-$ ). Buffering anions can modulate the local pH by acting as a proton source, thus affecting the selectivity of  $\text{H}_2$  and methane ( $\text{CH}_4$ ) whose rate-determining steps (RDSS) involve the participation of protons.<sup>107,113–116</sup> Compared with non-buffering anions, the local pH would not change dramatically in buffering electrolytes ( $\text{HCO}_3^-$  or  $\text{H}_2\text{PO}_4^-$ ), preferentially facilitating the production of  $\text{CH}_4$  and  $\text{H}_2$ .<sup>117</sup> Particularly, the phosphate anions showed negligible activity towards  $\text{C}_{2+}$  products and largely favored the formation of  $\text{H}_2$  (FE > 70%) and  $\text{CH}_4$ . Besides, increasing the concentration of  $\text{HCO}_3^-$  from 0.05 to 0.2 M could enhance partial current densities of  $\text{H}_2$  and  $\text{CH}_4$ . Resasco *et al.* ascribed the above enhancement to the  $\text{p}K_a$  of the buffering anions.<sup>118</sup> The equilibrium constant for the deprotonation of  $\text{HCO}_3^-$  is  $10^4$  times higher than that for the deprotonation of  $\text{H}_2\text{O}$ , proving that  $\text{HCO}_3^-$  could supply its own protons to the electrode surface. Furthermore, upon decreasing the  $\text{p}K_a$  of buffering anions, the reaction rates for producing  $\text{H}_2$  and  $\text{CH}_4$  increases in the sequence  $\text{HCO}_3^-$  ( $\text{p}K_a = 10.33$ ) <  $\text{H}_3\text{BO}_3$  ( $\text{p}K_a = 9.23$ ) <  $\text{H}_2\text{PO}_4^-$  ( $\text{p}K_a = 7.21$ ). Thus, this substantially low  $\text{p}K_a$  of phosphate anions may account for the high selectivity of  $\text{H}_2$  as well.

In buffering anions,  $\text{HCO}_3^-$  also acts as a carbon source.<sup>119</sup> Through analyzing the CO product from the isotopically labelled  $^{13}\text{CO}_2$  reduction reaction in the  $\text{NaH}^{12}\text{CO}_3$  electrolytes, 89% of the CO product was  $^{12}\text{CO}$  (Fig. 5a). Moreover, surface adsorbed  $\text{CO}_2$  molecules were also from the  $\text{HCO}_3^-$  anions at the start of the reaction, observed by the real-time ATR-SEIRAS.<sup>120</sup> In light of the above results, it is clear that the vast majority of adsorbed  $\text{CO}_2$  molecules are from  $\text{HCO}_3^-$  rather than the freely dissolved  $\text{CO}_2$  molecules. Meanwhile, such a rapid equilibrium between  $\text{HCO}_3^-$  and dissolved  $\text{CO}_2$  molecules increased the effective concentration of  $\text{CO}_2$  near the electrode surface, hence boosting the rate of CO production (Fig. 5b). Moreover, Shan *et al.* noted that  $\text{HCO}_3^-$  could improve the stability of the intermediate  $^*\text{OOC}^-$  on the surface, hence facilitating the formation of this intermediate and further formate.<sup>121</sup>

In terms of non-buffering anions, the formed higher local pH gave better selectivity to ethylene ( $\text{C}_2\text{H}_4$ ) (> 45%) and total  $\text{C}_{2+}$  products (> 65%). Especially for halide anions of  $\text{Cl}^-$ ,  $\text{Br}^-$  and  $\text{I}^-$ , they could specifically adsorb on the surface of

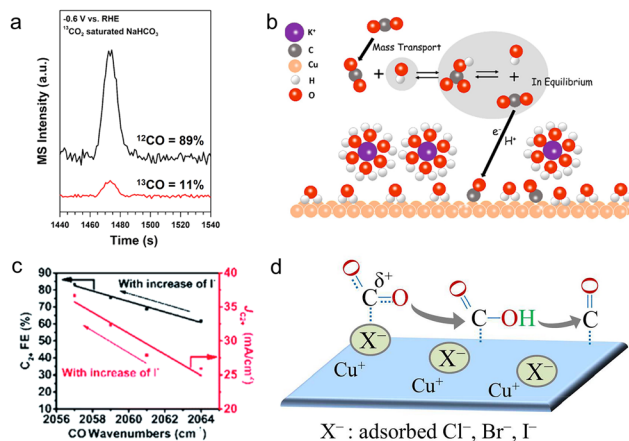


Fig. 5 (a) The mass spectra of the CO product under  $-0.6$  V vs. RHE in the  $^{13}\text{CO}_2$  saturated  $\text{NaH}^{12}\text{CO}_3$  electrolyte.<sup>119</sup> Reproduced from ref. 119 with permission from the American Chemical Society, copyright 2017. (b) The schematic of the proposed mechanism for providing  $\text{CO}_2$  molecules from  $\text{HCO}_3^-$ .<sup>120</sup> Reproduced from ref. 120 with permission from the American Chemical Society, copyright 2017. (c) Variation of FE and current density of  $\text{C}_{2+}$  with CO wavenumbers as the concentration of  $\text{I}^-$  varies.<sup>126</sup> Reproduced from ref. 126 with permission from the Royal Society of Chemistry, copyright 2022. (d) Illustration of the improvement in the adsorption of  $\text{CO}_2$  and the stabilization of the intermediate  $^*\text{CO}$  in the presence of halides.<sup>123</sup> Reproduced from ref. 123 with permission from the American Chemical Society, copyright 2017.

catalysts, changing surface morphologies and surface charges during the  $\text{CO}_2\text{RR}$ .<sup>122–124</sup> According to the DFT calculations, the specific halide adsorption is increasingly favorable in the order  $\text{Cl}^- < \text{Br}^- < \text{I}^-$  on a well-defined Cu surface.<sup>122</sup> In the meantime, the enhanced adsorption ability of halides will affect the negative charge transfer of adsorbed halides to the Cu surface. Hence, compared with  $\text{Cl}^-$  and  $\text{Br}^-$ , a more negative charge of  $\text{I}^-$  could be readily transferred to the Cu surface, modifying the local electronic environment.<sup>125</sup> This further improves the interactions between Cu and the intermediates  $^*\text{CO}_2$  and  $^*\text{CO}$ , thus promoting the protonation of  $^*\text{CO}$  and further forming  $\text{CH}_4$ . Consequently, the presence of  $\text{I}^-$  impedes the CO production and enhances the  $\text{CH}_4$  selectivity 6 times higher compared with the halide-free (potassium bicarbonate ( $\text{KHCO}_3$ )) electrolyte. Besides, the specific adsorption of halide anions may lead to the transfer of their negative charges to the intermediates  $^*\text{CO}$ , giving rise to the stronger adsorption of  $^*\text{CO}$  and further faster C–C coupling kinetics. This was demonstrated by the decrease of the wavenumbers of CO with increasing concentration of halide anions using *in situ* ATR-SEIRAS, and a higher  $\text{C}_{2+}$  FE of 84.5% was achieved (Fig. 5c).<sup>126</sup>

Different from the above results, Dunfeng *et al.* noted that the addition of halides had a minor effect on the selectivity of all products, but mainly increased the reaction rates and positively shifted the onset potentials for forming  $\text{C}_2$  products, following the trend no halide <  $\text{Cl}^- < \text{Br}^- < \text{I}^-$  in the mixed electrolytes containing 0.1 M  $\text{KHCO}_3$  and 0.3 M  $\text{KX}$  ( $\text{X} = \text{Cl}$ ,  $\text{Br}$ , and  $\text{I}$ ).<sup>123</sup> Such improvement may result from the effect of halides on the common step for the generation of all products. As shown in Fig. 5d, the specifically adsorbed halide formed a

covalent  $X^-$ -C bond with a local  $\text{CO}_2$  molecule by donating its partial charge to the carbon atom. This further changed the linear form of  $\text{CO}_2$  to the bent species, thereby facilitating the adsorption of  $\text{CO}_2$  and stabilizing the intermediate  $^*\text{COOH}$ . Moreover, while the specific adsorption of halides led to the nanostructuring of the Cu surface, especially  $\text{I}^-$ , the observed similar current densities among halides demonstrated that the surface morphology differences could not account for the change in activity.

Unlike the above effects of halides on the  $\text{CO}_2\text{RR}$  in mixed solutions, the FE of  $\text{C}_2$  products could be greatly enhanced in the halide-only electrolytes with the sequence of  $\text{ClO}_4^- < \text{Cl}^- < \text{Br}^- < \text{I}^-$ .<sup>127</sup> The ethylene and ethanol FEs increased from 31% and 7% ( $\text{ClO}_4^-$ ) to 50% and 16% ( $\text{I}^-$ ), and the associated current densities increased five and seven times, respectively. By using linear sweep voltammetry, a higher population of  $^*\text{CO}$  adsorbed on the surface was observed in the presence of  $\text{I}^-$ , thus promoting the C-C coupling to  $\text{C}_2$  products. A similar effect was also found on the zinc (Zn) electrodes in the  $\text{CO}_2\text{RR}$ .<sup>128</sup> In comparison with the FE of CO (~13%) in the  $\text{KHCO}_3$  solution, a four times higher CO selectivity (~48%) was achieved in the KCl electrolyte.

Hydroxide anions also favor the reduction of  $\text{CO}_2$  to  $\text{C}_{2+}$  products and a high ethylene FE of 70% at  $-0.55$  V vs. RHE was obtained on the GDE.<sup>28</sup> According to the DFT calculations, the  $\text{OH}^-$  tended to lower the binding energy of the intermediate  $^*\text{CO}$ . Meanwhile, by increasing the charge imbalance between carbon atoms in the adsorbed intermediate  $^*\text{OCCO}$ , the  $\text{OH}^-$  could greatly stabilize this intermediate. Thus, the combined effects could reduce the energy barrier for the  $^*\text{CO}$  coupling, significantly increasing the formation of  $\text{C}_{2+}$  products, especially ethylene.

## 5. Conclusions and outlook

In this review, we presented the development of an EDL model and discussed the effects of different species in the electrolytes on the properties of the EDL, and thus on the activity and selectivity for the  $\text{CO}_2\text{RR}$ . The solvated cations, adsorbed at the interface, could stabilize the intermediates including  $^*\text{CO}_2$  and  $^*\text{OCCO}$  through coordination. Meanwhile, the accumulation of cations at the OHP would enhance the interfacial electric field, favoring the stabilization of intermediates with larger dipole moments. Besides, the  $\text{p}K_a$  values varying with the sizes of cations affect the local pH and the concentration of  $\text{CO}_2$ , and further product selectivity. In addition, the effects of different anions on the activity and selectivity for the  $\text{CO}_2\text{RR}$  were also discussed.

Apart from the investigation on the mechanisms of the cation effect, researchers have developed different strategies to leverage this effect. Based on the DFT calculations, the adsorbed  $\text{K}^+$  can lower the thermodynamic energy barrier for the conversion of  $\text{CO}_2$  to CO on Au electrodes.<sup>129</sup> Sargent *et al.* managed to significantly improve the concentration of  $\text{K}^+$  near the electrode by using the Au nanoneedles that produce high local electric fields,

resulting in an order of magnitude improvement in performance compared to other Au electrodes with different morphologies. Besides, in the acidic systems, the perfluorosulfonic acid ionomer has also been used to concentrate the  $\text{K}^+$  on the catalyst surface, which could increase the  $\text{C}_{2+}$  selectivity by the electrostatic interactions of  $\text{K}^+$  with specific adsorbates.<sup>92</sup> At a current density of  $1.2$  A  $\text{cm}^{-2}$ , 61% of the  $\text{CO}_2\text{RR}$  selectivity including 40% FE of  $\text{C}_{2+}$  products was achieved. On the other hand, because of having a compact EDL,  $\text{K}^+$  has also been introduced to improve the electron transfer from the electrode to carbamate and the adsorption energy of reactants, further promoting the conversion of  $\text{CO}_2$  captured by amine-based chemical solvents.<sup>130</sup>

On the other hand, *in situ* spectroscopies including SEIRAS and surface-enhanced Raman spectroscopy (SERS) have often been employed to explore the reaction interface and mechanisms of the  $\text{CO}_2\text{RR}$ .<sup>131-133</sup> Both *in situ* studies aim at identifying the identity and configuration of intermediates during the  $\text{CO}_2\text{RR}$ , and their evolution as a function of electrode potential, electrolyte composition and other parameters. Hence, this will vastly assist researchers in investigating the reaction pathways and the effect of reaction environments (especially ions in the EDL). In our review, SEIRAS can be used to probe the local pH and observe a dynamic equilibrium between bicarbonate and dissolved  $\text{CO}_2$ , and investigate the interaction between cations and the adsorbed intermediate  $^*\text{CO}$ . However, for other intermediates, it is considerably hard to detect and confirm their identity, owing to their short residual time and low coverage on the surface. To address this issue, combining SEIRAS and online mass spectroscopy or other instruments which are capable of identifying products will be a possible and challenging strategy. Developing stabilizers and trapping reagents for stabilizing or capturing intermediates might be another way to further understand the mechanism.

Despite the development of *in situ* spectroscopies, there are still plenty of issues that need to be addressed. In most instances, the catalyst surface is more complicated to study experimentally than theoretically. Such complexity will lead to changes in the local cation distribution and the interfacial electric field and its strength. It is not clear to what extent the catalyst surface will severely affect the cation distribution and the field. Furthermore, the degree of cation hydration and the impact of cations on the structure of water molecules in the hydration shell or the interfacial water molecules and thus on the interactions between intermediates and cations/water molecules warrant further investigation.

## Conflicts of interest

There are no conflicts to declare.

## Acknowledgements

This work acknowledges the funding support from the National Natural Science Foundation of China (52103300), Guangdong

Basic and Applied Basic Research Foundation (2023A1515010572), and the Shenzhen Science and Technology Program (JCYJ20210324132806017 and GXWD20220811163904001).

## References

1 Y. Y. Birdja, E. Pérez-Gallent, M. C. Figueiredo, A. J. Göttle, F. Calle-Vallejo and M. T. M. Koper, Advances and challenges in understanding the electrocatalytic conversion of carbon dioxide to fuels, *Nat. Energy*, 2019, **4**, 732–745.

2 S. Nitopi, E. Bertheussen, S. B. Scott, X. Liu, A. K. Engstfeld, S. Horch, B. Seger, I. E. L. Stephens, K. Chan, C. Hahn, J. K. Nørskov, T. F. Jaramillo and I. Chorkendorff, Progress and Perspectives of Electrochemical CO<sub>2</sub> Reduction on Copper in Aqueous Electrolyte, *Chem. Rev.*, 2019, **119**, 7610–7672.

3 N. S. Spinner, J. A. Vega and W. E. Mustain, Recent progress in the electrochemical conversion and utilization of CO<sub>2</sub>, *Catal. Sci. Technol.*, 2012, **2**, 19–28.

4 D. D. Zhu, J. L. Liu and S. Z. Qiao, Recent Advances in Inorganic Heterogeneous Electrocatalysts for Reduction of Carbon Dioxide, *Adv. Mater.*, 2016, **28**, 3423–3452.

5 T. Zheng, K. Jiang and H. Wang, Recent Advances in Electrochemical CO<sub>2</sub>-to-CO Conversion on Heterogeneous Catalysts, *Adv. Mater.*, 2018, **30**, 1802066.

6 J. Yu, J. Wang, Y. Ma, J. Zhou, Y. Wang, P. Lu, J. Yin, R. Ye, Z. Zhu and Z. Fan, Recent Progresses in Electrochemical Carbon Dioxide Reduction on Copper-Based Catalysts toward Multicarbon Products, *Adv. Funct. Mater.*, 2021, **31**, 2102151.

7 M.-G. Kim, J. Park, Y. Choi, H. C. Song, S.-H. Kim, K.-M. Bang, H. C. Ham, N.-K. Kim, D. H. Won, B. K. Min, S. J. Yoo and W. Kim, CuIr Nanoparticles for Electrochemical Reduction of CO<sub>2</sub> to t-BuOH, *Adv. Energy Mater.*, 2023, 2300749.

8 R. Reske, H. Mistry, F. Behafarid, B. Roldan Cuenya and P. Strasser, Particle Size Effects in the Catalytic Electrocatalytic Reduction of CO<sub>2</sub> on Cu Nanoparticles, *J. Am. Chem. Soc.*, 2014, **136**, 6978–6986.

9 J. L. Wang, H. Y. Tan, Y. P. Zhu, H. Chu and H. M. Chen, Linking the Dynamic Chemical State of Catalysts with the Product Profile of Electrocatalytic CO<sub>2</sub> Reduction, *Angew. Chem., Int. Ed.*, 2021, **60**, 17254–17267.

10 Z. Z. Wu, F. Y. Gao and M. R. Gao, Regulating the oxidation state of nanomaterials for electrocatalytic CO<sub>2</sub> reduction, *Energy Environ. Sci.*, 2021, **14**, 1121–1139.

11 W. J. Luo, X. W. Nie, M. J. Janik and A. Asthagiri, Facet Dependence of CO<sub>2</sub> Reduction Paths on Cu Electrodes, *ACS Catal.*, 2016, **6**, 219–229.

12 J. L. Qiao, Y. Y. Liu, F. Hong and J. J. Zhang, A review of catalysts for the electroreduction of carbon dioxide to produce low-carbon fuels, *Chem. Soc. Rev.*, 2014, **43**, 631–675.

13 R. Dorakhan, I. Grigioni, B.-H. Lee, P. Ou, J. Abed, C. O'Brien, A. Sedighian Rasouli, M. Plodinec, R. K. Miao, E. Shirzadi, J. Wicks, S. Park, G. Lee, J. Zhang, D. Sinton and E. H. Sargent, A silver–copper oxide catalyst for acetate electrosynthesis from carbon monoxide, *Nat. Synth.*, 2023, **2**, 448–457.

14 X. Wang, P. F. Ou, A. Ozden, S. F. Hung, J. Tam, C. M. Gabardo, J. Y. Howe, J. Sisler, K. Bertens, F. P. G. de Arquer, R. K. Miao, C. P. O'Brien, Z. Y. Wang, J. Abed, A. S. Rasouli, M. J. Sun, A. H. Ip, D. Sinton and E. H. Sargent, Efficient electrosynthesis of n-propanol from carbon monoxide using a Ag-Ru-Cu catalyst, *Nat. Energy*, 2022, **7**, 170–176.

15 J. Gu, C.-S. Hsu, L. Bai, H. M. Chen and X. Hu, Atomically dispersed Fe<sup>3+</sup> sites catalyze efficient CO<sub>2</sub> electroreduction to CO, *Science*, 2019, **364**, 1091–1094.

16 S. Lin, C. S. Diercks, Y.-B. Zhang, N. Kornienko, E. M. Nichols, Y. Zhao, A. R. Paris, D. Kim, P. Yang, O. M. Yaghi and C. J. Chang, Covalent organic frameworks comprising cobalt porphyrins for catalytic CO<sub>2</sub> reduction in water, *Science*, 2015, **349**, 1208–1213.

17 W. Zhu, Y.-J. Zhang, H. Zhang, H. Lv, Q. Li, R. Michalsky, A. A. Peterson and S. Sun, Active and Selective Conversion of CO<sub>2</sub> to CO on Ultrathin Au Nanowires, *J. Am. Chem. Soc.*, 2014, **136**, 16132–16135.

18 D. Gao, H. Zhou, J. Wang, S. Miao, F. Yang, G. Wang, J. Wang and X. Bao, Size-Dependent Electrocatalytic Reduction of CO<sub>2</sub> over Pd Nanoparticles, *J. Am. Chem. Soc.*, 2015, **137**, 4288–4291.

19 S. He, F. Ni, Y. Ji, L. Wang, Y. Wen, H. Bai, G. Liu, Y. Zhang, Y. Li, B. Zhang and H. Peng, The p-Orbital Delocalization of Main-Group Metals to Boost CO<sub>2</sub> Electroreduction, *Angew. Chem., Int. Ed.*, 2018, **57**, 16114–16119.

20 Y. Zhou, R. Zhou, X. Zhu, N. Han, B. Song, T. Liu, G. Hu, Y. Li, J. Lu and Y. Li, Mesoporous PdAg Nanospheres for Stable Electrochemical CO<sub>2</sub> Reduction to Formate, *Adv. Mater.*, 2020, **32**, 2000992.

21 T. Zheng, C. Liu, C. Guo, M. Zhang, X. Li, Q. Jiang, W. Xue, H. Li, A. Li, C.-W. Pao, J. Xiao, C. Xia and J. Zeng, Copper-catalysed exclusive CO<sub>2</sub> to pure formic acid conversion via single-atom alloying, *Nat. Nanotechnol.*, 2021, **16**, 1386–1393.

22 X. Y. Cao, L. L. Zhao, B. R. Wulan, D. X. Tan, Q. W. Chen, J. Z. Ma and J. T. Zhang, Atomic Bridging Structure of Nickel-Nitrogen-Carbon for Highly Efficient Electrocatalytic Reduction of CO<sub>2</sub>, *Angew. Chem., Int. Ed.*, 2022, **61**, e2021139.

23 Y. Wang, Z. Wang, C.-T. Dinh, J. Li, A. Ozden, M. Golam Kibria, A. Seifitokaldani, C.-S. Tan, C. M. Gabardo, M. Luo, H. Zhou, F. Li, Y. Lum, C. McCallum, Y. Xu, M. Liu, A. Proppe, A. Johnston, P. Todorovic, T.-T. Zhuang, D. Sinton, S. O. Kelley and E. H. Sargent, Catalyst synthesis under CO<sub>2</sub> electroreduction favours faceting and promotes renewable fuels electrosynthesis, *Nat. Catal.*, 2020, **3**, 98–106.

24 H. Huo, J. Wang, Q. Fan, Y. Hu and J. Yang, Cu-MOFs Derived Porous Cu Nanoribbons with Strengthened Electric Field for Selective CO<sub>2</sub> Electroreduction to C<sup>2+</sup> Fuels, *Adv. Energy Mater.*, 2021, **11**, 2102447.

25 Z. Gu, H. Shen, Z. Chen, Y. Yang, C. Yang, Y. Ji, Y. Wang, C. Zhu, J. Liu, J. Li, T.-K. Sham, X. Xu and G. Zheng, Efficient Electrocatalytic  $\text{CO}_2$  Reduction to  $\text{CO}_2$  Alcohols at Defect-Site-Rich Cu Surface, *Joule*, 2021, **5**, 429–440.

26 D. M. Weekes, D. A. Salvatore, A. Reyes, A. Huang and C. P. Berlinguette, Electrolytic  $\text{CO}_2$  Reduction in a Flow Cell, *Acc. Chem. Res.*, 2018, **51**, 910–918.

27 C. M. Gabardo, C. P. O'Brien, J. P. Edwards, C. McCallum, Y. Xu, C.-T. Dinh, J. Li, E. H. Sargent and D. Sinton, Continuous Carbon Dioxide Electroreduction to Concentrated Multi-carbon Products Using a Membrane Electrode Assembly, *Joule*, 2019, **3**, 2777–2791.

28 C.-T. Dinh, T. Burdyny, M. G. Kibria, A. Seifitokaldani, C. M. Gabardo, F. P. García de Arquer, A. Kiani, J. P. Edwards, P. De Luna, O. S. Bushuyev, C. Zou, R. Quintero-Bermudez, Y. Pang, D. Sinton and E. H. Sargent,  $\text{CO}_2$  electroreduction to ethylene via hydroxide-mediated copper catalysis at an abrupt interface, *Science*, 2018, **360**, 783–787.

29 K. Qi, Y. Zhang, N. Onofrio, E. Petit, X. Cui, J. Ma, J. Fan, H. Wu, W. Wang, J. Li, J. Liu, Y. Zhang, Y. Wang, G. Jia, J. Wu, L. Lajaunie, C. Salameh and D. Voiry, Unlocking direct  $\text{CO}_2$  electrolysis to C3 products via electrolyte supersaturation, *Nat. Catal.*, 2023, **6**, 319–331.

30 M. G. Kibria, J. P. Edwards, C. M. Gabardo, C. T. Dinh, A. Seifitokaldani, D. Sinton and E. H. Sargent, Electrochemical  $\text{CO}_2$  Reduction into Chemical Feedstocks: From Mechanistic Electrocatalysis Models to System Design, *Adv. Mater.*, 2019, **31**, 1807166.

31 D. Wakerley, S. Lamaison, J. Wicks, A. Clemens, J. Feaster, D. Corral, S. A. Jaffer, A. Sarkar, M. Fontecave, E. B. Duoss, S. Baker, E. H. Sargent, T. F. Jaramillo and C. Hahn, Gas diffusion electrodes, reactor designs and key metrics of low-temperature  $\text{CO}_2$  electrolyzers, *Nat. Energy*, 2022, **7**, 130–143.

32 C. Xia, P. Zhu, Q. Jiang, Y. Pan, W. Liang, E. Stavitski, H. N. Alshareef and H. Wang, Continuous production of pure liquid fuel solutions via electrocatalytic  $\text{CO}_2$  reduction using solid-electrolyte devices, *Nat. Energy*, 2019, **4**, 776–785.

33 R. Kortlever, J. Shen, K. J. P. Schouten, F. Calle-Vallejo and M. T. M. Koper, Catalysts and Reaction Pathways for the Electrochemical Reduction of Carbon Dioxide, *J. Phys. Chem. Lett.*, 2015, **6**, 4073–4082.

34 M. E. Leonard, L. E. Clarke, A. Forner-Cuenca, S. M. Brown and F. R. Brushett, Investigating Electrode Flooding in a Flowing Electrolyte, Gas-Fed Carbon Dioxide Electrolyzer, *ChemSusChem*, 2020, **13**, 400–411.

35 M. Duarte, B. De Mot, J. Hereijgers and T. Breugelmans, Electrochemical Reduction of  $\text{CO}_2$ : Effect of Convective  $\text{CO}_2$  Supply in Gas Diffusion Electrodes, *ChemElectroChem*, 2019, **6**, 5596–5602.

36 S. Verma, Y. Hamasaki, C. Kim, W. Huang, S. Lu, H.-R. M. Jhong, A. A. Gewirth, T. Fujigaya, N. Nakashima and P. J. A. Kenis, Insights into the Low Overpotential Electro-reduction of  $\text{CO}_2$  to CO on a Supported Gold Catalyst in an Alkaline Flow Electrolyzer, *ACS Energy Lett.*, 2018, **3**, 193–198.

37 Y. J. Sa, C. W. Lee, S. Y. Lee, J. Na, U. Lee and Y. J. Hwang, Catalyst-electrolyte interface chemistry for electrochemical  $\text{CO}_2$  reduction, *Chem. Soc. Rev.*, 2020, **49**, 6632–6665.

38 J. Chen and L. Wang, Effects of the Catalyst Dynamic Changes and Influence of the Reaction Environment on the Performance of Electrochemical  $\text{CO}_2$  Reduction, *Adv. Mater.*, 2022, **34**, 2103900.

39 S.-J. Shin, D. H. Kim, G. Bae, S. Ringe, H. Choi, H.-K. Lim, C. H. Choi and H. Kim, On the importance of the electric double layer structure in aqueous electrocatalysis, *Nat. Commun.*, 2022, **13**, 174.

40 G. Gonella, E. H. G. Backus, Y. Nagata, D. J. Bonthuis, P. Loche, A. Schlaich, R. R. Netz, A. Kühnle, I. T. McCrum, M. T. M. Koper, M. Wolf, B. Winter, G. Meijer, R. K. Campen and M. Bonn, Water at charged interfaces, *Nat. Rev. Chem.*, 2021, **5**, 466–485.

41 L. R. F. Allen and J. Bard, *Electrochemical Methods: Fundamentals and Applications*, Wiley, 2nd edn, 2000.

42 H. Helmholtz, Ueber einige Gesetze der Vertheilung elektrischer Ströme in körperlichen Leitern mit Anwendung auf die thierisch-elektrischen Versuche, *Ann. Phys.*, 1853, **165**, 211–233.

43 M. Gouy, Sur la constitution de la charge électrique à la surface d'un électrolyte, *J. Phys. Theor. Appl.*, 1910, **9**, 457–468.

44 D. L. Chapman, LI. A contribution to the theory of electrocapillarity, *London Edinburgh Philos. Mag. J. Sci.*, 1913, **25**, 475–481.

45 O. Stern, Zur Theorie Der Elektrolytischen Doppelschicht, *Z. Elektrochem. Angew. Phys. Chem.*, 1924, **30**, 508–516.

46 D. C. Grahame, The Electrical Double Layer and the Theory of Electrocapillarity, *Chem. Rev.*, 1947, **41**, 441–501.

47 M. M. Waegele, C. M. Gunathunge, J. Li and X. Li, How cations affect the electric double layer and the rates and selectivity of electrocatalytic processes, *J. Chem. Phys.*, 2019, **151**, 160902.

48 M. Dunwell, Y. Yan and B. Xu, Understanding the influence of the electrochemical double-layer on heterogeneous electrochemical reactions, *Curr. Opin. Chem. Eng.*, 2018, **20**, 151–158.

49 M. Moura de Salles Pupo and R. Kortlever, Electrolyte Effects on the Electrochemical Reduction of  $\text{CO}_2$ , *ChemPhysChem*, 2019, **20**, 2926–2935.

50 M. König, J. Vaes, E. Klemm and D. Pant, Solvents and Supporting Electrolytes in the Electrocatalytic Reduction of  $\text{CO}_2$ , *iScience*, 2019, **19**, 135–160.

51 S. J. Shin, H. Choi, S. Ringe, D. H. Won, H. S. Oh, D. H. Kim, T. Lee, D. H. Nam, H. Kim and C. H. Choi, A unifying mechanism for cation effect modulating C1 and C2 productions from  $\text{CO}_2$  electroreduction, *Nat. Commun.*, 2022, **13**, 5482.

52 W. Paik, T. N. Andersen and H. Eyring, Kinetic studies of the electrolytic reduction of carbon dioxide on the mercury electrode, *Electrochim. Acta*, 1969, **14**, 1217–1232.

53 A. Murata and Y. Hori, Product Selectivity Affected by Cationic Species in Electrochemical Reduction of  $\text{CO}_2$

and CO at a Cu Electrode, *Bull. Chem. Soc. Jpn.*, 1991, **64**, 123–127.

54 M. C. O. Monteiro, F. Dattila, N. López and M. T. M. Koper, The Role of Cation Acidity on the Competition between Hydrogen Evolution and CO<sub>2</sub> Reduction on Gold Electrodes, *J. Am. Chem. Soc.*, 2022, **144**, 1589–1602.

55 S. Banerjee, X. Han and V. S. Thoi, Modulating the Electrode-Electrolyte Interface with Cationic Surfactants in Carbon Dioxide Reduction, *ACS Catal.*, 2019, **9**, 5631–5637.

56 M. R. Singh, Y. Kwon, Y. Lum, J. W. Ager, III and A. T. Bell, Hydrolysis of Electrolyte Cations Enhances the Electrochemical Reduction of CO<sub>2</sub> over Ag and Cu, *J. Am. Chem. Soc.*, 2016, **138**, 13006–13012.

57 L. D. Chen, M. Urushihara, K. Chan and J. K. Nørskov, Electric Field Effects in Electrochemical CO<sub>2</sub> Reduction, *ACS Catal.*, 2016, **6**, 7133–7139.

58 M. C. O. Monteiro, F. Dattila, B. Hagedoorn, R. García-Muelas, N. López and M. T. M. Koper, Absence of CO<sub>2</sub> electroreduction on copper, gold and silver electrodes without metal cations in solution, *Nat. Catal.*, 2021, **4**, 654–662.

59 J. Gu, S. Liu, W. Ni, W. Ren, S. Haussener and X. Hu, Modulating electric field distribution by alkali cations for CO<sub>2</sub> electroreduction in strongly acidic medium, *Nat. Catal.*, 2022, **5**, 268–276.

60 Y. Hori and S. Suzuki, Electrolytic Reduction of Carbon Dioxide at Mercury Electrode in Aqueous Solution, *Bull. Chem. Soc. Jpn.*, 1982, **55**, 660–665.

61 A. N. Frumkin, Influence of cation adsorption on the kinetics of electrode processes, *Trans. Faraday Soc.*, 1959, **55**, 156–167.

62 S. A. Akhade, I. T. McCrum and M. J. Janik, The Impact of Specifically Adsorbed Ions on the Copper-Catalyzed Electroreduction of CO<sub>2</sub>, *J. Electrochem. Soc.*, 2016, **163**, F477.

63 M. R. Thorson, K. I. Siil and P. J. A. Kenis, Effect of Cations on the Electrochemical Conversion of CO<sub>2</sub> to CO, *J. Electrochem. Soc.*, 2013, **160**, F69.

64 V. J. Ovalle, Y. S. Hsu, N. Agrawal, M. J. Janik and M. M. Waegele, Correlating hydration free energy and specific adsorption of alkali metal cations during CO<sub>2</sub> electroreduction on Au, *Nat. Catal.*, 2022, **5**, 624–632.

65 D. Strmenik, K. Kodama, D. van der Vliet, J. Greeley, V. R. Stamenkovic and N. M. Marković, The role of non-covalent interactions in electrocatalytic fuel-cell reactions on platinum, *Nat. Chem.*, 2009, **1**, 466–472.

66 J. N. Mills, I. T. McCrum and M. J. Janik, Alkali cation specific adsorption onto fcc(111) transition metal electrodes, *Phys. Chem. Chem. Phys.*, 2014, **16**, 13699–13707.

67 M. R. Singh, E. L. Clark and A. T. Bell, Effects of electrolyte, catalyst, and membrane composition and operating conditions on the performance of solar-driven electrochemical reduction of carbon dioxide, *Phys. Chem. Chem. Phys.*, 2015, **17**, 18924–18936.

68 O. Ayemoba and A. Cuesta, Spectroscopic Evidence of Size-Dependent Buffering of Interfacial pH by Cation Hydrolysis during CO<sub>2</sub> Electroreduction, *ACS Appl. Mater. Interfaces*, 2017, **9**, 27377–27382.

69 F. Zhang and A. C. Co, Direct Evidence of Local pH Change and the Role of Alkali Cation during CO<sub>2</sub> Electroreduction in Aqueous Media, *Angew. Chem., Int. Ed.*, 2020, **59**, 1674–1681.

70 X. Liu, M. C. O. Monteiro and M. T. M. Koper, Interfacial pH measurements during CO<sub>2</sub> reduction on gold using a rotating ring-disk electrode, *Phys. Chem. Chem. Phys.*, 2023, **25**, 2897–2906.

71 A. S. Malkani, J. Anibal and B. Xu, Cation Effect on Interfacial CO<sub>2</sub> Concentration in the Electrochemical CO<sub>2</sub> Reduction Reaction, *ACS Catal.*, 2020, **10**, 14871–14876.

72 F. Che, J. T. Gray, S. Ha, N. Kruse, S. L. Scott and J.-S. McEwen, Elucidating the Roles of Electric Fields in Catalysis: A Perspective, *ACS Catal.*, 2018, **8**, 5153–5174.

73 J. Resasco, L. D. Chen, E. Clark, C. Tsai, C. Hahn, T. F. Jaramillo, K. Chan and A. T. Bell, Promoter Effects of Alkali Metal Cations on the Electrochemical Reduction of Carbon Dioxide, *J. Am. Chem. Soc.*, 2017, **139**, 11277–11287.

74 H. Y. Yu, S. E. Weitzner, J. B. Varley, B. C. Wood and S. A. Akhade, Surface Engineering of Copper Catalyst through CO\* Adsorbate, *J. Phys. Chem. C*, 2023, **127**, 1789–1797.

75 E. Pérez-Gallent, G. Marcandalli, M. C. Figueiredo, F. Calle-Vallejo and M. T. M. Koper, Structure- and Potential-Dependent Cation Effects on CO Reduction at Copper Single-Crystal Electrodes, *J. Am. Chem. Soc.*, 2017, **139**, 16412–16419.

76 S. Ringe, E. L. Clark, J. Resasco, A. Walton, B. Seger, A. T. Bell and K. Chan, Correction: Understanding cation effects in electrochemical CO<sub>2</sub> reduction, *Energy Environ. Sci.*, 2019, **12**, 3609–3610.

77 D. Bohra, J. H. Chaudhry, T. Burdyny, E. A. Pidko and W. A. Smith, Modeling the electrical double layer to understand the reaction environment in a CO<sub>2</sub> electrocatalytic system, *Energy Environ. Sci.*, 2019, **12**, 3380–3389.

78 C. M. Gunathunge, V. J. Ovalle and M. M. Waegele, Probing promoting effects of alkali cations on the reduction of CO at the aqueous electrolyte/copper interface, *Phys. Chem. Chem. Phys.*, 2017, **19**, 30166–30172.

79 M. Nakamura, Y. Nakajima, K. Kato, O. Sakata and N. Hoshi, Surface Oxidation of Au(111) Electrode in Alkaline Media Studied by Using X-ray Diffraction and Infrared Spectroscopy: Effect of Alkali Metal Cation on the Alcohol Oxidation Reactions, *J. Phys. Chem. C*, 2015, **119**, 23586–23591.

80 C. A. Lucas, P. Thompson, Y. Gründer and N. M. Markovic, The structure of the electrochemical double layer: Ag(111) in alkaline electrolyte, *Electrochim. Commun.*, 2011, **13**, 1205–1208.

81 D. K. Lambert, Vibrational Stark effect of adsorbates at electrochemical interfaces, *Electrochim. Acta*, 1996, **41**, 623–630.

82 A. S. Malkani, J. Li, N. J. Oliveira, M. He, X. Chang, B. Xu and Q. Lu, Understanding the electric and nonelectric field components of the cation effect on the electrochemical CO reduction reaction, *Sci. Adv.*, 2020, **6**, eabd2569.

83 J. Li, D. Wu, A. S. Malkani, X. Chang, M.-J. Cheng, B. Xu and Q. Lu, Hydroxide Is Not a Promoter of  $C_{2+}$  Product Formation in the Electrochemical Reduction of CO on Copper, *Angew. Chem., Int. Ed.*, 2020, **59**, 4464–4469.

84 X. P. Qin, T. Vegge and H. A. Hansen, Cation-Coordinated Inner-Sphere  $CO_2$  Electroreduction at Au-Water Interfaces, *J. Am. Chem. Soc.*, 2023, **145**, 1897–1905.

85 H. Liu, J. Liu and B. Yang, Promotional Role of a Cation Intermediate Complex in  $C_2$  Formation from Electrochemical Reduction of  $CO_2$  over Cu, *ACS Catal.*, 2021, **11**, 12336–12343.

86 M. Ma, K. Djanashvili and W. A. Smith, Controllable Hydrocarbon Formation from the Electrochemical Reduction of  $CO_2$  over Cu Nanowire Arrays, *Angew. Chem., Int. Ed.*, 2016, **55**, 6680–6684.

87 X. Y. Chen, J. F. Chen, N. M. Alghoraibi, D. A. Henckel, R. X. Zhang, U. O. Nwabara, K. E. Madsen, P. J. A. Kenis, S. C. Zimmerman and A. A. Gewirth, Electrochemical  $CO_2$ -to-ethylene conversion on polyamine-incorporated Cu electrodes, *Nat. Catal.*, 2021, **4**, 20–27.

88 J. A. Rabinowitz and M. W. Kanan, The future of low-temperature carbon dioxide electrolysis depends on solving one basic problem, *Nat. Commun.*, 2020, **11**, 5231.

89 C. Chen, Y. Li and P. Yang, Address the “alkalinity problem” in  $CO_2$  electrolysis with catalyst design and translation, *Joule*, 2021, **5**, 737–742.

90 M. Ma, E. L. Clark, K. T. Therkildsen, S. Dalsgaard, I. Chorkendorff and B. Seger, Insights into the carbon balance for  $CO_2$  electroreduction on Cu using gas diffusion electrode reactor designs, *Energy Environ. Sci.*, 2020, **13**, 977–985.

91 M. C. O. Monteiro, M. F. Philips, K. J. P. Schouten and M. T. M. Koper, Efficiency and selectivity of  $CO_2$  reduction to CO on gold gas diffusion electrodes in acidic media, *Nat. Commun.*, 2021, **12**, 4943.

92 J. E. Huang, F. Li, A. Ozden, A. Sedighian Rasouli, F. P. García de Arquer, S. Liu, S. Zhang, M. Luo, X. Wang, Y. Lum, Y. Xu, K. Bertens, R. K. Miao, C.-T. Dinh, D. Sinton and E. H. Sargent,  $CO_2$  electrolysis to multicarbon products in strong acid, *Science*, 2021, **372**, 1074–1078.

93 S. Ringe, C. G. Morales-Guio, L. D. Chen, M. Fields, T. F. Jaramillo, C. Hahn and K. Chan, Double layer charging driven carbon dioxide adsorption limits the rate of electrochemical carbon dioxide reduction on Gold, *Nat. Commun.*, 2020, **11**, 33.

94 Y. Xie, P. F. Ou, X. Wang, Z. Y. Xu, Y. C. Li, Z. Y. Wang, J. E. Huang, J. Wicks, C. McCallum, N. Wang, Y. H. Wang, T. X. Chen, B. T. W. Lo, D. Sinton, J. C. Yu, Y. Wang and E. H. Sargent, High carbon utilization in  $CO_2$  reduction to multi-carbon products in acidic media, *Nat. Catal.*, 2022, **5**, 564–570.

95 H. Li, H. Li, P. Wei, Y. Wang, Y. Zang, D. Gao, G. Wang and X. Bao, Tailoring acidic microenvironments for carbon-efficient  $CO_2$  electrolysis over a Ni-N-C catalyst in a membrane electrode assembly electrolyzer, *Energy Environ. Sci.*, 2023, **16**, 1502–1510.

96 I. Ledezma-Yanez, W. D. Z. Wallace, P. Sebastián-Pascual, V. Climent, J. M. Feliu and M. T. M. Koper, Interfacial water reorganization as a pH-dependent descriptor of the hydrogen evolution rate on platinum electrodes, *Nat. Energy*, 2017, **2**, 17031.

97 C. J. Bondue, M. Graf, A. Goyal and M. T. M. Koper, Suppression of Hydrogen Evolution in Acidic Electrolytes by Electrochemical  $CO_2$  Reduction, *J. Am. Chem. Soc.*, 2021, **143**, 279–285.

98 A. Goyal, G. Marcandalli, V. A. Mints and M. T. M. Koper, Competition between  $CO_2$  Reduction and Hydrogen Evolution on a Gold Electrode under Well-Defined Mass Transport Conditions, *J. Am. Chem. Soc.*, 2020, **142**, 4154–4161.

99 H. Ooka, M. C. Figueiredo and M. T. M. Koper, Competition between Hydrogen Evolution and Carbon Dioxide Reduction on Copper Electrodes in Mildly Acidic Media, *Langmuir*, 2017, **33**, 9307–9313.

100 H. G. Qin, F. Z. Li, Y. F. Du, L. F. Yang, H. Wang, Y. Y. Bai, M. Lin and J. Gu, Quantitative Understanding of Cation Effects on the Electrochemical Reduction of  $CO_2$  and  $H^+$  in Acidic Solution, *ACS Catal.*, 2023, **13**, 916–926.

101 Z. Y. Xu, M. Z. Sun, Z. S. Zhang, Y. Xie, H. S. Hou, X. B. Ji, T. F. Liu, B. L. Huang and Y. Wang, Steering the Selectivity of Electrochemical  $CO_2$  Reduction in Acidic Media, *ChemCatChem*, 2022, **14**, e202200052.

102 Y. Qiao, W. Lai, K. Huang, T. Yu, Q. Wang, L. Gao, Z. Yang, Z. Ma, T. Sun, M. Liu, C. Lian and H. Huang, Engineering the Local Microenvironment over Bi Nanosheets for Highly Selective Electrocatalytic Conversion of  $CO_2$  to  $HCOOH$  in Strong Acid, *ACS Catal.*, 2022, **12**, 2357–2364.

103 J. Li, X. Li, C. M. Gunathunge and M. M. Waegele, Hydrogen bonding steers the product selectivity of electrocatalytic CO reduction, *Proc. Natl. Acad. Sci. U. S. A.*, 2019, **116**, 9220–9229.

104 A. Schizodimou and G. Kyriacou, Acceleration of the reduction of carbon dioxide in the presence of multivalent cations, *Electrochim. Acta*, 2012, **78**, 171–176.

105 S. S. Bhargava, E. R. Cofell, P. Chumble, D. Azmoodeh, S. Someshwar and P. J. A. Kenis, Exploring multivalent cations-based electrolytes for  $CO_2$  electroreduction, *Electrochim. Acta*, 2021, **394**, 139055.

106 A. Seifitokaldani, C. M. Gabardo, T. Burdyny, C.-T. Dinh, J. P. Edwards, M. G. Kibria, O. S. Bushuyev, S. O. Kelley, D. Sinton and E. H. Sargent, Hydronium-Induced Switching between  $CO_2$  Electroreduction Pathways, *J. Am. Chem. Soc.*, 2018, **140**, 3833–3837.

107 A. Bagger, L. Arnarson, M. H. Hansen, E. Spohr and J. Rossmeisl, Electrochemical CO Reduction: A Property of the Electrochemical Interface, *J. Am. Chem. Soc.*, 2019, **141**, 1506–1514.

108 F. Quan, M. Xiong, F. Jia and L. Zhang, Efficient electroreduction of  $CO_2$  on bulk silver electrode in aqueous solution via the inhibition of hydrogen evolution, *Appl. Surf. Sci.*, 2017, **399**, 48–54.

109 S. Banerjee, X. Han and V. S. Thoi, Modulating the Electrode-Electrolyte Interface with Cationic Surfactants

in Carbon Dioxide Reduction, *ACS Catal.*, 2019, **9**, 5631–5637.

110 W. X. Ge, Y. X. Chen, Y. Fan, Y. H. Zhu, H. L. Liu, L. Song, Z. Liu, C. Lian, H. L. Jiang and C. Z. Li, Dynamically Formed Surfactant Assembly at the Electrified Electrode-Electrolyte Interface Boosting CO<sub>2</sub> Electroreduction, *J. Am. Chem. Soc.*, 2022, **144**, 6613–6622.

111 Z.-Q. Zhang, S. Banerjee, V. S. Thoi and A. Shoji Hall, Reorganization of Interfacial Water by an Amphiphilic Cationic Surfactant Promotes CO<sub>2</sub> Reduction, *J. Phys. Chem. Lett.*, 2020, **11**, 5457–5463.

112 S. Banerjee, Z. Q. Zhang, A. S. Hall and V. S. Thoi, Surfactant Perturbation of Cation Interactions at the Electrode-Electrolyte Interface in Carbon Dioxide Reduction, *ACS Catal.*, 2020, **10**, 9907–9914.

113 M. N. Jackson, O. Jung, H. C. Lamotte and Y. Surendranath, Donor-Dependent Promotion of Interfacial Proton-Coupled Electron Transfer in Aqueous Electrocatalysis, *ACS Catal.*, 2019, **9**, 3737–3743.

114 A. S. Varela, M. Kroschel, T. Reier and P. Strasser, Controlling the selectivity of CO<sub>2</sub> electroreduction on copper: The effect of the electrolyte concentration and the importance of the local pH, *Catal. Today*, 2016, **260**, 8–13.

115 M. Schreier, Y. Yoon, M. N. Jackson and Y. Surendranath, Competition between H and CO for Active Sites Governs Copper-Mediated Electrosynthesis of Hydrocarbon Fuels, *Angew. Chem., Int. Ed.*, 2018, **57**, 10221–10225.

116 Y. Chen, C. W. Li and M. W. Kanan, Aqueous CO<sub>2</sub> Reduction at Very Low Overpotential on Oxide-Derived Au Nanoparticles, *J. Am. Chem. Soc.*, 2012, **134**, 19969–19972.

117 Y. Hori, A. Murata and R. Takahashi, Formation of hydrocarbons in the electrochemical reduction of carbon dioxide at a copper electrode in aqueous solution, *J. Chem. Soc., Faraday Trans. 1*, 1989, **85**, 2309–2326.

118 J. Resasco, Y. Lum, E. Clark, J. Z. Zeledon and A. T. Bell, Effects of Anion Identity and Concentration on Electrochemical Reduction of CO<sub>2</sub>, *ChemElectroChem*, 2018, **5**, 1064–1072.

119 M. Dunwell, Q. Lu, J. M. Heyes, J. Rosen, J. G. Chen, Y. Yan, F. Jiao and B. Xu, The Central Role of Bicarbonate in the Electrochemical Reduction of Carbon Dioxide on Gold, *J. Am. Chem. Soc.*, 2017, **139**, 3774–3783.

120 S. Zhu, B. Jiang, W.-B. Cai and M. Shao, Direct Observation on Reaction Intermediates and the Role of Bicarbonate Anions in CO<sub>2</sub> Electrochemical Reduction Reaction on Cu Surfaces, *J. Am. Chem. Soc.*, 2017, **139**, 15664–15667.

121 W. Y. Shan, R. Liu, H. C. Zhao and J. F. Liu, Bicarbonate Rebalances the \*COOH/\*OCO- Dual Pathways in CO<sub>2</sub> Electrocatalytic Reduction: In Situ Surface-Enhanced Raman Spectroscopic Evidence, *J. Phys. Chem. Lett.*, 2022, **13**, 7296–7305.

122 I. T. McCrum, S. A. Akhade and M. J. Janik, Electrochemical specific adsorption of halides on Cu 111, 100, and 211: A Density Functional Theory study, *Electrochim. Acta*, 2015, **173**, 302–309.

123 D. Gao, F. Scholten and B. Roldan Cuenya, Improved CO<sub>2</sub> Electroreduction Performance on Plasma-Activated Cu Catalysts via Electrolyte Design: Halide Effect, *ACS Catal.*, 2017, **7**, 5112–5120.

124 S. Lee, D. Kim and J. Lee, Electrocatalytic Production of C<sub>3</sub>-C<sub>4</sub> Compounds by Conversion of CO<sub>2</sub> on a Chloride-Induced Bi-Phasic Cu<sub>2</sub>O-Cu Catalyst, *Angew. Chem., Int. Ed.*, 2015, **54**, 14701–14705.

125 A. S. Varela, W. Ju, T. Reier and P. Strasser, Tuning the Catalytic Activity and Selectivity of Cu for CO<sub>2</sub> Electroreduction in the Presence of Halides, *ACS Catal.*, 2016, **6**, 2136–2144.

126 T. H. Yuan, T. Wang, G. Zhang, W. Y. Deng, D. F. Cheng, H. Gao, J. Zhao, J. Yu, P. Zhang and J. L. Gong, The effect of specific adsorption of halide ions on electrochemical CO<sub>2</sub> reduction, *Chem. Sci.*, 2022, **13**, 8117–8123.

127 Y. Huang, C. W. Ong and B. S. Yeo, Effects of Electrolyte Anions on the Reduction of Carbon Dioxide to Ethylene and Ethanol on Copper (100) and (111) Surfaces, *ChemSusChem*, 2018, **11**, 3299–3306.

128 M. Zhao, H. Tang, Q. Yang, Y. Gu, H. Zhu, S. Yan and Z. Zou, Inhibiting Hydrogen Evolution using a Chloride Adlayer for Efficient Electrochemical CO<sub>2</sub> Reduction on Zn Electrodes, *ACS Appl. Mater. Interfaces*, 2020, **12**, 4565–4571.

129 M. Liu, Y. Pang, B. Zhang, P. De Luna, O. Voznyy, J. Xu, X. Zheng, C. T. Dinh, F. Fan, C. Cao, F. P. G. de Arquer, T. S. Safaei, A. Mepham, A. Klinkova, E. Kumacheva, T. Filleteer, D. Sinton, S. O. Kelley and E. H. Sargent, Enhanced electrocatalytic CO<sub>2</sub> reduction via field-induced reagent concentration, *Nature*, 2016, **537**, 382–386.

130 G. Lee, Y. C. Li, J.-Y. Kim, T. Peng, D.-H. Nam, A. Sedighian Rasouli, F. Li, M. Luo, A. H. Ip, Y.-C. Joo and E. H. Sargent, Electrochemical upgrade of CO<sub>2</sub> from amine capture solution, *Nat. Energy*, 2021, **6**, 46–53.

131 Y. W. Choi, H. Mistry and B. Roldan Cuenya, New insights into working nanostructured electrocatalysts through operando spectroscopy and microscopy, *Curr. Opin. Electrochem.*, 2017, **1**, 95–103.

132 A. D. Handoko, F. X. Wei, Jenndy, B. S. Yeo and Z. W. Seh, Understanding heterogeneous electrocatalytic carbon dioxide reduction through operando techniques, *Nat. Catal.*, 2018, **1**, 922–934.

133 S. Q. Zhu, T. H. Li, W. B. Cai and M. H. Shao, CO<sub>2</sub> Electrochemical Reduction As Probed through Infrared Spectroscopy, *ACS Energy Lett.*, 2019, **4**, 682–689.